2015 International Symposium on Nonlinear Theory and its Applications
NOLTA2015, Kowloon, Hong Kong, China, December 1-4, 2015

Initial-State Dependence of the Route to Chaos in a High-Dimensional Dynamical System: External-Cavity Semiconductor Lasers

Byungchil Kim †‡, A. Locquet‡†, Daeyoung Choi†‡, and D. S. Citrin†‡

†Georgia Institute of Technology, School of Electrical and Computer Engineering, Atlanta, Georgia 30332-0250 USA
‡UMI 2958 Georgia Tech-CNRS, Georgia Tech Lorraine, 2 Rue Marconi F-57070, Metz, France
Email: alexandre@gatech.edu, korea@gatech.edu

Abstract—We observe experimentally for the first time, in a high-dimensional dynamical system experiencing generalized multistability, the sensitivity of the route to chaos to the selection of the initial state. This demonstration is performed using a semiconductor laser subjected to external optical feedback from an external mirror for which we developed an experimental initial-state selection method. We observe that, as the feedback level is increased, depending on the initial state, chaos develops from a different mode of the external-cavity.

1. Introduction

External-cavity semiconductor lasers (ECLs) utilize an external cavity formed by a mirror to provide time-delayed optical feedback into the gain region of the laser diode (LD). ECLs are known to display various dynamical behaviors depending on the operating and device parameters. It is, for example, known that the delayed feedback produces an infinite-dimensional dynamical system–the infinite dimensions are due to the infinite number of initial conditions needed to specify the subsequent dynamics of a differential-delay system–in which hundreds of attractors or attractor ruins can coexist, leading to a wealth of dynamical regimes of varying complexity [1]. Thus, ECLs have become a classical paradigm for generating high-speed (subnanosecond) chaotic fluctuations in high-dimensional time-delayed dynamical systems [2]. Their highly complex dynamics further make them attractive for applications as diverse as chaos communications [3] and ultrahigh rate random-bit generation [4].

Despite years of interest in these systems, experimental investigations on ECLs have suffered from a lack of detailed and systematic experimental knowledge of the various dynamical regimes that can be accessed as a function of the various operating parameters, such as the feedback strength η, the current I injected into the laser, and the external-cavity length L, which in turn determines the system delay $\tau = 2L/c$ with c the speed of light. A standard tool for analyzing the dynamical regimes of a complex nonlinear system is the bifurcation diagram (BD), which maps out the dynamical regimes as a parameter of the system is continuously tuned. The BD is a plot of the histogram of local extrema of a dynamical quantity as a single parameter of the system is varied; transitions between qualitatively different dynamical regimes, known as bifurcations, are evident in the BD, and the sequence of bifurcations in a system that eventually exhibits chaos is known as the route to chaos.

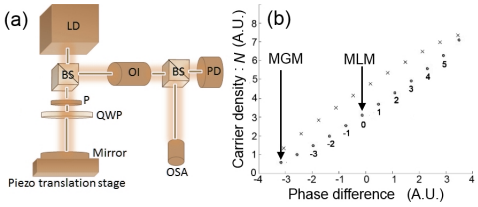

Figure 1: (a) Experimental setup. LD: laser diode, BS: beam splitter, PD: photodetector, P : polarizer, QWP : quarter-wave plate, OI : Optical isolator, OSA : Optical spectrum analyzer. (b) Ellipse structure of fixed points in the phase-difference-vs.-N plane. Circles represent stable external-cavity modes; crosses represent unstable antimodes. The labels indicate the mode number.

In this study, we report a clear *experimental* dependence on initial conditions of the route to chaos in a distributed feedback laser (DFB) ECL biased at $I \sim (2\text{–}3)I_{th}$ in the long-cavity case, in which, L is chosen such that the relaxation-oscillation frequency f_{RO} is higher than the external-cavity free-spectral range $f_\tau = \tau^{-1}$. To do so, we select the initial external cavity mode on which the laser operates at low η and map out the forward BD.

2. Experimental setup and theoretical background

The experimental setup is shown in Fig. 1(a) and was described in Ref. [5]. A real-time oscilloscope is used to capture the time-dependence of the optical output intensity $\mathcal{I}(t)$. We also measure the spectrum of $\mathcal{I}(t)$ (RF spectrum) with a spectrum analyzer and the optical spectrum with a high-resolution optical spectrum analyzer. In all cases, we choose $L = 30$ cm, corresponding to $\tau = 2$ ns, amply satisfying the long-cavity criterion. The feedback strength η, controlled by the reflection associated with the external cavity that is allowed to propagate back into the laser, is varied via the angle of the quarter-wave plate (QWP) in the feedback loop. Maximum feedback, corresponding to $\eta = 1$, is

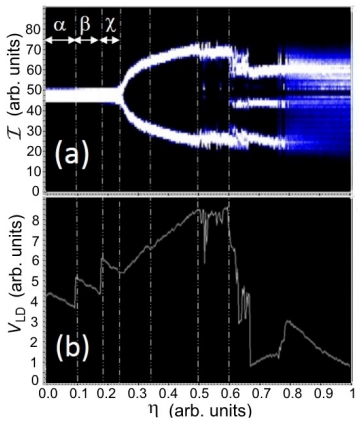

Figure 2: (a) Reverse BD for $I = 22.59$ mA and $L = 30$ cm and (b) the corresponding $V_{\rm LD}$.

reached when the QWP angle is such that electric field is not subjected to any rotation. In that case, ∼20 % of the optical power is fed back onto the collimating lens.

It is well-known that the delayed optical feedback has a profound impact on the dynamics of the ECL and that it leads to the creation of two types of CW modes: potentially stable external-cavity modes ECMs, separated in frequency by approximately f_τ, and unstable antimodes [6]. Moreover, according to the widely-used Lang and Kobayashi model [7], the ECMs and antimodes lie on an ellipse in the carrier density N versus phase difference $\Delta\phi(t) = \phi(t) - \phi(t-\tau)$ plane projected from the three-dimensional phase space $(N, \mathcal{I}, \phi)$, as shown in Fig. 1(b). Among ECMs, two stand out: the minimum linewidth mode (MLM) and the maximum gain mode (MGM). The MGM is the one with the lowest frequency (high-gain end of the ellipse), and is usually stable [6, 8]. The MLM is the closest ECM in frequency to the solitary LD mode. The evolution of the system can be visualized in terms of the trajectory moving amongst the ECMs and antimodes lying on this ellipse.

3. Initial-state dependence of the route to chaos

In numerical simulations, one simply chooses initial conditions and computes from there. In experiment, however, this can be quite challenging. A typical example of the reverse BD is shown in Fig. 2(a) and the corresponding $V_{\rm LD}$ is shown in Fig. 2(b). It has been shown [9] that $V_{\rm LD}$ tracks the changes in the time-averaged N. One observes two discontinuities in $V_{\rm LD}$ at $\eta = 0.1$ and 0.18 [Fig. 2(b)]. These discontinuties reveal that different ECMs are participating in the light emission for regions α, β, and χ. As will be discussed later, the discontinuities in $V_{\rm LD}$ can be correlated with the changes in the optical spectrum, which evidence first a shift from ECM 2 to 1, followed by a shift from ECM 1 to 0 as η is ramped from 0.24 down to 0: Fig.

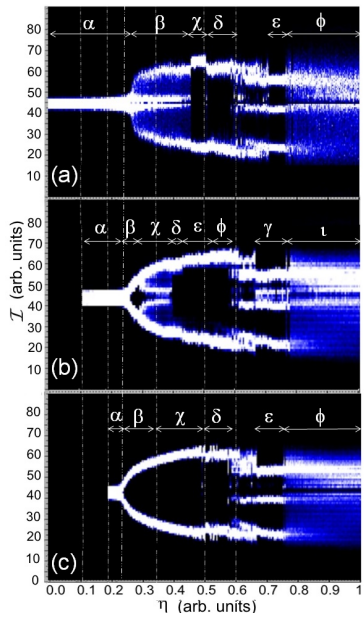

Figure 3: Forward BDs for several initial conditions for I = 22.59 mA and L = 30 cm; Initial mode: (a) ECM 0, (b) ECM 1, and (c) ECM 2.

4(a) corresponds to Fig. 2 α , Fig. 5(a) to Fig. 2 β, and Fig. 6(a) to Fig. 2 χ.

Having illustrated the ability to detect the relevant ECM dominating the emission at low feedback levels, in Fig. 3(a),(b), and (c) we show forward BDs beginning on *different* ECMs (ECMs 0,1, and 2, respectively). The way we access different initial states is by ramping η *down* to a low value and then using this as the initial state from which we map out the forward BD. Though the lowest η reached in the three BDs is different, the three BDs overlap for η belonging to the interval [0.18,1]. As a result, in this interval, all the system parameters (*including* feedback phase) are identical except for the initial state of the ECL at $\eta = 0.18$. *As a result, the three BDs represent three different routes to fully developed CC of the same ECL starting from three different initial states.* The difference [see Fig. 3] among the three BDs starting from different ECMs is found to be significant in the sense that the route to chaos does depend on the initial state, as will be illustrated below.

Figure 3 (a) shows the forward BD starting from ECM 0, and Fig. 4 shows the corresponding optical spectrum. It is clear from the optical spectrum that in region α of Figs. 3(a) only one ECM (ECM 0) of the solitary laser (MLM) participates to the dynamics. As shown in Fig. 3(a), this stable mode survives over a large feedback interval ($\eta < 0.24$) and remains in a CW regime. When η is increased above that level, the optical spectrum [Fig. 4(b)] reveals that several ECMs (-3 to 3) start to participate in the emission. An analysis of the corresponding $\mathcal{I}(t)$ (not shown here), shows that the dynamical behavior is of a quasi-periodic nature.

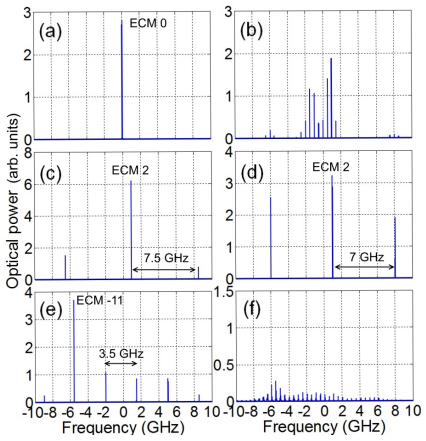

Figure 4: Optical spectrum with the initial condition ECM 0 for (a) $\eta = 0$, (b) 0.35, (c) 0.39, (d) 0.45, (e) 0.75, and (f) 0.9.

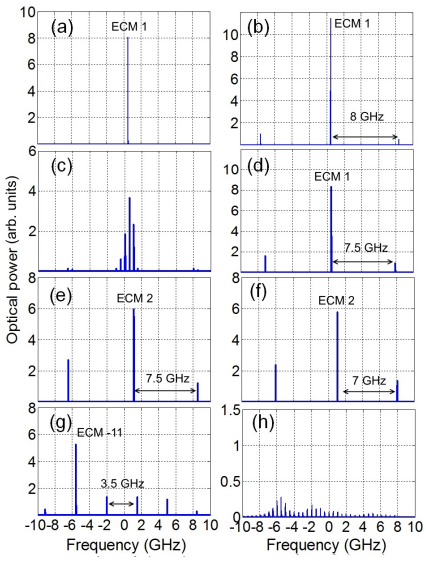

Figure 5: Optical spectrum with the initial condition ECM 1 for (a) $\eta = 0.15$, (b) 0.24, (c) 0.35, (d) 0.42, (e) 0.47, (f) 0.55, (g) 0.75, and (h) 0.9.

For a further increase in η (around 0.47), a discontinuity appears in the BD [region χ of Figs. 3(a)] that corresponds to an abrupt change of the dynamical behavior toward a limit-cycle oscillation. The optical spectrum [Fig. 4(c)] shows that the oscillation occurs around ECM 2, and the frequency of the oscillation 7.5 GHz as it corresponds to the distance between ECM 2 and its sidebands.

As we further increase η, at ~ 0.5, another limit cycle oscillating at $f_{RO} \sim 7$ GHz is observed [region δ of Fig. 3(a)]. The optical spectrum of Fig. 4(d) further confirms that the oscillation is manifested as sidebands at around ± 7 GHz from ECM 2. Interestingly, the dominant mode (ECM 2) does not change in the transition from region χ to δ of Fig. 3(a), indicating two different frequencies at 7.5 GHz and 7 GHz on ECM 2. Previous works [2] show that our observation of two limit cycles with different frequencies around the same ECM is compatible with the LK prediction.

For a further increase in η, at ~ 0.6, intermittency between the dynamical behaviors of regions δ and ϵ of Fig. 3(a) is observed.

Region ϵ, which corresponds to $\eta \gtrsim 0.74$, displays a periodic oscillation with a fundamental frequency of ~ 3.5 GHz and a harmonic at ~ 7 GHz, centered around ECM -11 [Fig. 4(e)]. The presence of the harmonic indicates that the 3.5 GHz limit cycle originates probably from a period-doubling bifurcation of a 7 GHz cycle that must have existed, at lower η, around ECM-11.

If η is further increased, the limit-cycle oscillation disappears, giving rise to fully-developed CC, (region ϕ) which involves multiple ECMs negatively-shifted in frequency [Fig. 4 (f)].

Figure 3(b) shows the forward BD starting from ECM 1 and Fig. 5 shows the corresponding optical spectrum. As expected, the ECL initially displays CW behavior [Fig. 5(a)] (region α ($\eta \sim 0.22$) of Fig. 3(b)] because only one fixed point (ECM 1) participates in the output. As η is increased above 0.22, it is clearly seen in the BD that the ECL undergoes a periodic oscillation. This oscillation is manifested as sidebands ± 8 GHz from ECM 1 [Fig. 5 (b)].

With increasing η, additional sidebands near $\pm f_\tau$ appear in the optical spectrum [Fig. 5(c)], revealing the presence of a second frequency in the dynamics. The undamping of a second frequency close to f_τ corresponds to a second Hopf bifurcation and signals the development, in phase space, of a torus attractor. Note that both the limit cycle and the torus result from the destabilization of ECM 1 and are located around it in phase space [Figs. 5(b),(c)].

For a further increase in η, another limit cycle appears in the BD. The optical spectrum shows [Fig. 5(d)] that this cycle is still centered on ECM 1, and has now a frequency of approximately ± 7.5 GHz. One notes that the dominant ECM 1 does not change in between Figs. 5(b) and (d), thus providing experimental evidence of the existence, at different η, around the same ECM, of two periodic solutions with different frequencies, 8 GHz and 7.5 GHz, whose separation is $\sim f_\tau$. As η is further increased, and region ϵ of Fig. 3(b) is reached, a small discontinuity is observed in the BD. The optical spectrum [Fig. 5(e)] reveals that this discontinuity corresponds to a shift from ECM 1 to 2. The ECL still oscillates periodically, and the optical spectrum confirms that the frequency of the oscillations is still 7.5 GHz. Increasing η yet further, another limit cycle at $f_{RO} \sim 7$ GHz is seen [region ϕ of Figs. 3(b)]. The active ECM 2 does not change in the transition from region ε to ϕ of Fig. 3(b), indicating again the existence of two different oscillation frequencies, 7.5 GHz and 7 GHz, again separated by $\sim f_\tau$ around a single ECM.

As η is increased even further, the scenario is similar to

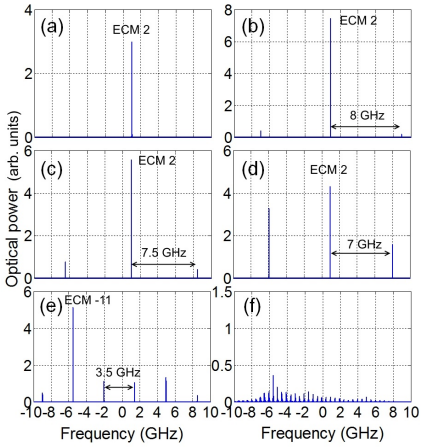

Figure 6: Optical spectrum with the initial condition ECM 2 for (a) $\eta = 0.2$, (b) 0.3, (c) 0.39, (d) 0.55, (e) 0.7, and (f) 0.9.

the one observed for Fig. 3(a): the trajectory moves toward negatively-shifted ECMS: first, a period-doubled limit cycle around ECM -11 is observed (region γ) and then a regime of fully-developed CC (region η).

Figure 3(c) shows the forward BD starting from ECM 2 and Fig. 6 the corresponding optical spectrum. In the initial region α ($\eta \sim 0.22$) of Fig. 3(c), only one fixed point (ECM 2) participates in the output, and the ECL displays a CW behavior [Fig. 6 (a)]. As η is increased above 0.22 and region β is reached, the ECL undergoes a periodic oscillation [Fig. 6 (b)], manifested as sidebands ±8 GHz from ECM 2. Increasing η, the optical spectrum reveals the existence of two regions, χ and δ, corresponding to the appearance of two other limit cycles, of frequencies ±7.5 GHz [Figs. 6 (c)] and ±7 GHz [Figs. 6 (d)], still centered on ECM 2. It is noteworthy that the active ECM (2) does not change between Figs. 6(b),(c), and (d), thus providing evidence of the existence, at different η, of three periodic solutions with different frequencies, 8 GHz, 7.5 GHz and 7 GHz, whose separation is $\sim f_\tau$. For larger feedback regions, the behavior of the BD is similar to that of the two previous cases.

4. Conclution

To conclude, we show that the initial conditions chosen have a profound impact on the route to chaos exhibited by ECLs otherwise sharing identical parameters. We note in particular that the qualitative behavior of the route to chaos changes considerably at small η; however, the chaotic windows in Figs. 3 (a), (b), and (c) are of roughly the same size and are reached from almost the same η. These observations can be interpreted by the fact that at moderately low η, various attractors have developed around several ECMS, but have not yet merged or only a few neighboring attractors have merged [10]. As as result, the system is an configuration of generalized muntistability in which the initial state will be crucial in determining the dynamics experienced by the ECL, confirming the predictions by [6]. For larger η, most attractors have merged and, independent of the initial state of the BD, the trajectories end being attracted by a group of merged attractor ruins located around ECMs with a large negative frequency detuning, as is typical in a regime of fully-developed CC. *To the best of our knowledge, these are also the first experimental observations of the sensitivity to initial conditions of the BD of a high-dimensional dynamical system experiencing generalized multistability.*

References

[1] Soriano *et al.*, "Complex photonics: Dynamics and applications of delay-coupled semiconductors lasers," *Rev. Mod. Phys.*, vol. 85, no. 1, pp. 421–470, 2013.

[2] J. Mork *et al.*, "Route to chaos and competition between relaxation oscillations for a semiconductor-laser with optical feedback," *Phy. Rev. Lett.*, vol. 65, no. 16, pp. 1999–2002, 1990.

[3] A. Argyris *et al.*, "Chaos-based communications at high bit rates using commercial fibre-optic links," *Nature*, vol. 438, no. 7066, pp. 343–346, 2005.

[4] A. Uchida *et al.*, "Fast physical random bit generation with chaotic semiconductor lasers," *Nature Photon.*, vol. 2, no. 12, pp. 728–732, 2008.

[5] B. Kim *et al.*, "Experimental bifurcation-cascade diagram of an external-cavity semiconductor laser," *Opt. Express*, vol. 22, no. 3, pp. 2348–2357, 2014.

[6] C. Masoller and N. B. Abraham, "Stability and dynamical properties of the coexisting attractors of an external-cavity semiconductor laser," *Phys. Rev. A*, vol. 57, no. 2, pp. 1313–1322, 1998.

[7] R. Lang and K. Kobayashi, "External optical feedback effects on semiconductor injection-laser properties," *IEEE J. Quantum Electron.*, vol. 16, no. 3, pp. 347–355, 1980.

[8] T. Heil *et al.*, "Coexistence of low-frequency fluctuations and stable emission on a single high-gain mode in semiconductor lasers with external optical feedback," *Phys. Rev. A*, vol. 58, no. 4, pp. R2672–R2675, 1998.

[9] A. A. Sahai *et al.*, "Mapping the nonlinear dynamics of a laser diode via its terminal voltage," *Opt. Lett.*, vol. 39, no. 19, pp. 5630–5633, 2014.

[10] C. Masoller, "Coexistence of attractors in a laser diode with optical feedback from a large external cavity," *Phys. Rev. A*, vol. 50, pp. 2569–2578, 1994.